Cross-view Anchor Graph Learning and Factorization for Incomplete Multi-view Clustering

Xinxin Wang[1,3], Yongshan Zhang[2*], Xiaochen Yuan[4], Yicong Zhou[5]
[1]School of Artificial Intelligence, Shenzhen University
[2]School of Computer Science, China University of Geosciences
[3]Guangdong Provincial Key Laboratory of Intelligent Information Processing
[4]Faculty of Applied Sciences, Macau Polytechnic University
[5]Department of Computer and Information Science, University of Macau
xinxinwang1024@gmail.com, yszhang.cug@gmail.com, xcyuan@mpu.edu.mo, yicongzhou@um.edu.mo

Abstract

Graph-based incomplete multi-view clustering algorithms have gathered much attention due to their impressive clustering performance. However, existing methods primarily leverage intra-view correlation from observed views, while ignoring the exploration of explicit compensation relationships between different views. Moreover, these methods need post-processing to get labels, and the separate steps lack negotiation, which may lead to sub-optimal solutions. To address these issues, we propose a Cross-view Anchor Graph Learning and Factorization (AGLF) method. AGLF develops an Anchor Graph Completion (AGC) framework that explicitly learns the missing subgraph structures. Instead of requiring post-processing, AGC directly produces soft labels. By establishing a third-order tensor of soft labels, it employs the tensor Schatten p-norm to enhance anchor graph learning and factorization. To significantly improve the quality of subgraph learning, AGLF incorporates compensation subgraphs from supplementary views into the AGC framework, enabling the construction of a better anchor graph for label learning. An optimization algorithm is devised to solve the objective function. Experimental results across various datasets demonstrate the effectiveness of our method.

Introduction

Multi-view clustering exploits the consistent and complementary information among views to enhance clustering performance and have been extensively deployed in applications that have no label information (Hu, Shi, and Ye 2022; Qin et al. 2025). For example, they use hyperspectral and multispectral images to recognize land cover in earth observation (Wang, Zhang, and Zhou 2025c; Zhang et al. 2025b), as well as utilize textual information, click records, and user behavior logs to recommend news articles (Wang et al. 2021). However, existing multi-view clustering methods assume that all views of samples are complete. This assumption can be easily violated in real scenarios due to data corruption and equipment malfunction (Wen et al. 2023b; Liu et al. 2023). Therefore, when multi-view clustering approaches are directly applied to incomplete multi-view data, they often experience significant performance degradation or even complete failure. Consequently, Incomplete Multi-view Clustering (IMVC) has become a significant challenge.

To solve this problem, various solutions have been proposed in literature (Li et al. 2025; Qin and Qian 2024; Qin, Feng, and Zhang 2025). These existing incomplete clustering methods can be divided into three categories: representation-based, kernel-based, and graph-based. Representation-based IMVC methods typically transform the incomplete multi-view features into a unified representation. The work in (Wen et al. 2020b) utilized enhanced matrix factorization to obtain a unified latent embedding, on which K-mean is applied to yield final clustering results. The work in (Lin et al. 2021) applied contrastive learning to obtain discriminative presentation and clustering prediction. With the development of kernel technologies, many researchers developed IMVC methods based on kernel learning (Liu et al. 2019; Li et al. 2022a; Zhang et al. 2025a). These methods map all views into kernel space and then impute incomplete kernels for clustering. The third category of IMVC method involves the application of graph-based information to obtain clustering results (Cui et al. 2022; Li et al. 2022b, 2024c; Xia et al. 2022). These methods fuse multiple graphs to create a consensus graph, on which spectral clustering technologies are applied to obtain final clustering results. For example, Wen et al. proposed a subspace learning framework that uses tensor technologies to constrain graph learning (Wen et al. 2021). The works in (Wang, Zhang, and Zhou 2025a; Wen et al. 2023a) explored high-confidence information from the graph of each viewpoint to guide the learning of the consensus graph.

These aforementioned methods have achieved extensive success in IMVC. However, we observe that the complementary information in incomplete data is not adequately exploited. Furthermore, graph-based methods leverage only observed views for intra-view correlations of samples, ignoring the potential structural information for missing views. Additionally, most methods require separate post-processing to yield final clustering results, which may lead to sub-optimal outcomes. To address these problems, this paper proposes a Cross-view Anchor Graph Learning and Factorization (AGLF) method, which unifies cross-view imputation and clustering partition into a single optimization process and incorporates a low rank tensor constraint to cap-

*Corresponding author.

ture complementary information for improved partitioning. Specifically, since anchor graph can reduce the computational and storage burdens compared to full graph, we first construct an anchor graph for each view, filling in zero values for the elements missing from incomplete views. Then, inspired by the clustering efficiency of non-negative matrix factorization (Wang et al. 2025), we introduce an explicit subgraph matrix to fill the missing elements in anchor graph and decompose it to derive the clustering indicators. Meanwhile, a tensor Schatten p-norm is imposed on a third-order tensor constructed with indicator matrices to explore the complementary information. Finally, inspired by the potential information compensation from supplementary views, we construct supplementary view data for each view and use it to further enhance subgraph learning. The main contributions are summarized as follows:

- We propose an Anchor Graph Completion (AGC) framework, which unifies missing subgraph learning and graph decomposition in a unified model, incorporating a tensor Schatten p-norm on indicator tensor to enhance these processes.
- We construct supplementary view data matrices and utilize dynamic anchors to learn missing subgraphs, effectively exploring the compensation relationships between missing views and cross-view observed data.
- We propose an effective optimization algorithm to solve the objective function, which scales well with data size. Comprehensive experimental results clearly demonstrate the efficacy of the proposed AGLF method.

Related Work

Graph-based IMVC methods utilize graph structures to capture correlations among samples, applying clustering techniques to the fused consensus graph to derive final clustering results (Wen et al. 2020a). However, constructing a full graph from the entire original dataset can lead to redundant information and waste resources (Zhang et al. 2024). The anchor approach has emerged as an alternative and is gaining increasing attention (Liu et al. 2024). It first generates m representative data points $\mathbf{P}^{(\mathbf{v})} \in \mathbb{R}^{d_v \times m}$ from entire data $\mathbf{X}^{(\mathbf{v})} \in \mathbb{R}^{d_v \times n}$ to serve as anchors. Then, it constructs the anchor graph $\mathbf{E}^{(\mathbf{v})} \in \mathbb{R}^{m \times n}$ that characterizes the relationships between m anchors and n original data points. This significantly reduces computational and storage costs compared to a full graph, as $m \ll n$. Inspired by this, Wang et al. proposed an anchor graph-based IMVC method, IMVC-CBG (Wang et al. 2022). To adequately explore view information diversity, Liu et al. proposed FIMVC-VIA that utilizes view-independent anchors to learn a consensus anchor graph (Liu et al. 2022). Li et al. developed a parameter-free PSIMVC-PG method to enhance model practicability (Li et al. 2024b). To mitigate the randomness impact associated with heuristic anchors, (Chen et al. 2023) introduced dynamic anchor learning to improve model stability. To address the cross-view anchor misalignment problem, (Li et al. 2023) introduced a predefined anchor-level guiding graph to align dynamic anchors during learning process. The work RISE (Wang, Zhang, and Zhou 2025b) addressed the issue of rotational mismatch in the spectral embedding process of incomplete anchor graphs. Drawing on the outstanding representation learning capability of neural networks, CPSCAN leveraged the distribution calibration capability of anchors to enhance latent embedding alignment and imputation (Jin et al. 2023). The PMIMC work applied contrastive learning to strengthen anchors used for imputing missing data (Yuan et al. 2025). These methods have shown significant success, highlighting the substantial potential of anchors. However, they primarily focus on leveraging intra-view correlations of samples from observed views, neglecting the exploration of compensation relationships between different views.

Methodology

Notations

This section introduces the notations used throughout paper. We use bold calligraphy letters for third-order tensors, $\boldsymbol{\mathcal{F}} \in \mathbb{R}^{n_1 \times n_2 \times n_3}$, bold upper case letters for matrices, $\mathbf{F}$, bold lower case letters for vectors, $\mathbf{f}$, and lower case letters such as $f_{i,j}$ for the element in $\mathbf{F}$. We use $\boldsymbol{\mathcal{F}}^{(i)}$ to represent the i-th frontal slice of $\boldsymbol{\mathcal{F}}$. $\overline{\boldsymbol{\mathcal{F}}} = \text{fft}(\boldsymbol{\mathcal{F}}, [], 3)$ and $\boldsymbol{\mathcal{F}} = \text{ifft}(\overline{\boldsymbol{\mathcal{F}}}, [], 3)$ are the discrete Fourier transform (DFT) of $\boldsymbol{\mathcal{F}}$ along the third dimension and its reverse operation. Moreover, $\text{tr}(\mathbf{F})$ and $\mathbf{F}^{\mathrm{T}}$ stand for the trace and transpose of matrix $\mathbf{F}$. The F-norm of $\mathbf{F}$ is denoted by $\|\mathbf{F}\|_F$. To save space, we present only the definition of tensor Schatten p-norm; more definitions can be found in (Kilmer and Martin 2011).

Definition 1. (Gao et al. 2021) Given a third-order tensor $\boldsymbol{\mathcal{F}} \in \mathbb{R}^{n_1 \times n_2 \times n_3}$, the tensor Schatten p-th norm of $\boldsymbol{\mathcal{F}}$ is defined as

$$\|\boldsymbol{\mathcal{F}}\|_{\circledS}^p = \left(\sum_{i=1}^{n_3} \left\| \overline{\boldsymbol{\mathcal{F}}}^{(i)} \right\|_{\circledS}^p \right)^{\frac{1}{p}} = \left(\sum_{i=1}^{n_3} \sum_{j=1}^{\min(n_1,n_2)} \sigma_j \left(\overline{\boldsymbol{\mathcal{F}}}^{(i)} \right)^p \right)^{\frac{1}{p}} \tag{1}$$

where $\sigma_j \left(\overline{\boldsymbol{\mathcal{F}}}^{(i)} \right)$ is the j-th singular value of matrix $\overline{\boldsymbol{\mathcal{F}}}^{(i)}$, $0 < p \leq 1$. Recent researches show that when p is appropriately chosen, the Schatten p-norm provides an effective improvement for seeking tighter approximation of the rank function (Li et al. 2024a).

Proposed Formula

We first construct a local anchor graph from the observed features for each view, reducing computational and storage costs. Next, we aim to explicitly fill in the missing elements corresponding to the absent views and decompose the combined anchor graph to achieve the final clustering results. We formulate this process as an Anchor Graph Completion (AGC) framework:

$$\begin{aligned} \min_{\substack{a_v, \mathbf{M}_v \\ \mathbf{G}_v, \mathbf{F}_v}} & \sum_{v=1}^{V} a_v^2 \left\| \mathbf{E}_v + \mathbf{M}_v \mathbf{P}_v - \mathbf{G}_v \mathbf{F}_v^{\mathrm{T}} \right\|_F^2 + \lambda_1 \|\boldsymbol{\mathcal{F}}\|_{\circledS}^p \\ \text{s.t. } & \mathbf{M}_v^{\mathrm{T}} \mathbf{1} = \mathbf{1}, \mathbf{M}_v \geq 0, \mathbf{G}_v^{\mathrm{T}} \mathbf{G}_v = \mathbf{I}, \mathbf{F}_v \geq 0, \\ & \mathbf{a}^{\mathrm{T}} \mathbf{1} = \mathbf{1}, a_v \geq 0, \end{aligned} \tag{2}$$

where $\mathbf{E}_v \in \mathbb{R}^{m \times n}$ is an anchor graph constructed on incomplete data, with missing elements filled with zero val-

ues. $\mathbf{M}_v \in \mathbb{R}^{m\times n_v}$ represents missing information as a subgraph, with column normalization applied to avoid trivial solutions. $\mathbf{P}_v \in \{0,1\}^{n_v\times n}$ is an index matrix used to place the similarity elements of $\mathbf{M}_v$ into the missing positions. $\mathbf{G}_v \in \mathbb{R}^{m\times k}$ is a basis matrix, with an orthogonal constraint imposed to enhance the discriminability of the bases. $\mathbf{F}_v \in \mathbb{R}^{n\times k}$ is an indicator matrix. a_v is the view weight used to balance contributions from different views, and λ_1 is the trade-off parameter. Moreover, we stack matrices $\mathbf{F}_v$ into a third-order tensor as lateral slices and impose a tensor Schatten p-norm minimization constraint on $\boldsymbol{\mathcal{F}}$. This operation ensures a cross-view spatial low-rank structure for indicators of each sample, which effectively captures complementary information from different views.

In model (2), cross-view complementary information is explored solely on indicators using tensor learning, while subgraph information is inferred within view by minimizing data reconstruction loss. However, when the missing ratio is large, the limited observed information in the incomplete anchor graphs $\mathbf{E}_v$ may fail to effectively recover the missing data, leading to significant performance degradation. To address this problem, we propose to explicitly exploit the complementary information from data as follows:

$$\begin{aligned}\min_{\Omega} &\sum_{v=1}^{V} a_v^2 \left\|\mathbf{E}_v + \mathbf{M}_v\mathbf{P}_v - \mathbf{G}_v\mathbf{F}_v^{\mathrm{T}}\right\|_F^2 + \lambda_1 \left\|\boldsymbol{\mathcal{F}}\right\|_{\circledS p}^p \\ &+\lambda_2 \left\|\mathbf{W}_{\overline{v}}\mathbf{X}_{\overline{v}} - \mathbf{A}_v\mathbf{M}_v\right\|_F^2 \\ \text{s.t. } &\mathbf{M}_v^{\mathrm{T}}\mathbf{1} = \mathbf{1}, \mathbf{M}_v \geq 0, \mathbf{G}_v^{\mathrm{T}}\mathbf{G}_v = \mathbf{I}, \mathbf{F}_v \geq 0, \\ &\mathbf{a}^{\mathrm{T}}\mathbf{1} = \mathbf{1}, a_v \geq 0, \mathbf{W}_{\overline{v}}^{\mathrm{T}}\mathbf{W}_{\overline{v}} = \mathbf{I}, \mathbf{A}_v^{\mathrm{T}}\mathbf{A}_v = \mathbf{I},\end{aligned} \tag{3}$$

where $\Omega = \{a_v, \mathbf{M}_v, \mathbf{G}_v, \mathbf{F}_v, \mathbf{W}_{\overline{v}}, \mathbf{A}_v\}$ is a set of variables. $\overline{v}$ indicates the supplementary views of v-th view. $\mathbf{X}_{\overline{v}} \in \mathbb{R}^{d_{\overline{v}}\times n_v}$ represents the supplementary matrix for the v-th view, which concatenates the supplementary views along the column dimension. $\mathbf{W}_{\overline{v}} \in \mathbb{R}^{h\times d_{\overline{v}}}$ is a projection matrix that enhances feature discriminability. $\mathbf{A}_v \in \mathbb{R}^{h\times m}$ consists of dynamic anchors learned to disclose the clustering structure from complementary data. λ_2 is a trade-off parameter. The proposed third term leverages supplementary data across views to identify alternatives for missing information through dynamic anchor-based graph learning. It effectively expands the utilization of observed data by emphasizing inter-view information interaction.

Optimization

Inspired by Augmented Lagrange Multiplier (ALM), we introduce an auxiliary variable $\boldsymbol{\mathcal{J}}$, and let $\boldsymbol{\mathcal{J}} = \boldsymbol{\mathcal{F}}$. Then we rewrite the objective function as the following separable augmented Lagrange function:

$$\begin{aligned}\min_{\Omega} &\sum_{v=1}^{V} a_v^2 \left\|\mathbf{E}_v + \mathbf{M}_v\mathbf{P}_v - \mathbf{G}_v\mathbf{F}_v^{\mathrm{T}}\right\|_F^2 + \lambda_1 \left\|\boldsymbol{\mathcal{J}}\right\|_{\circledS p}^p \\ &+ \lambda_2 \left\|\mathbf{W}_{\overline{v}}\mathbf{X}_{\overline{v}} - \mathbf{A}_v\mathbf{M}_v\right\|_F^2 + \frac{\rho}{2}\|\boldsymbol{\mathcal{F}} - \boldsymbol{\mathcal{J}}\|_F^2 \\ &+ \langle \boldsymbol{\mathcal{Y}}, \boldsymbol{\mathcal{F}} - \boldsymbol{\mathcal{J}}\rangle \\ \text{s.t. } &\mathbf{M}_v^{\mathrm{T}}\mathbf{1} = \mathbf{1}, \mathbf{M}_v \geq 0, \mathbf{G}_v^{\mathrm{T}}\mathbf{G}_v = \mathbf{I}, \mathbf{F}_v \geq 0, \\ &\mathbf{a}^{\mathrm{T}}\mathbf{1} = \mathbf{1}, a_v \geq 0, \mathbf{W}_{\overline{v}}^{\mathrm{T}}\mathbf{W}_{\overline{v}} = \mathbf{I}, \mathbf{A}_v^{\mathrm{T}}\mathbf{A}_v = \mathbf{I},\end{aligned} \tag{4}$$

where $\Omega = \{a_v, \mathbf{M}_v, \mathbf{G}_v, \mathbf{F}_v, \boldsymbol{\mathcal{J}}, \mathbf{W}_{\overline{v}}, \mathbf{A}_v\}$ are variables to be solved. $\boldsymbol{\mathcal{Y}}$ is the Lagrange multiplier and $\rho > 0$ is the penalty parameter. Then, we can solve each variable individually while fixing the others.

Update $\mathbf{G}_v$ with fixed $\{a_v, \mathbf{M}_v, \mathbf{F}_v, \boldsymbol{\mathcal{J}}, \mathbf{W}_{\overline{v}}, \mathbf{A}_v\}$, Eq. (4) becomes:

$$\min_{\mathbf{G}_v^{\mathrm{T}}\mathbf{G}_v=\mathbf{I}} \left\|\mathbf{E}_v + \mathbf{M}_v\mathbf{P}_v - \mathbf{G}_v\mathbf{F}_v^{\mathrm{T}}\right\|_F^2 \tag{5}$$

which can be obviously written as:

$$\max_{\mathbf{G}_v^{\mathrm{T}}\mathbf{G}_v=\mathbf{I}} \mathrm{tr}\left(\mathbf{G}_v^{\mathrm{T}}(\mathbf{E}_v + \mathbf{M}_v\mathbf{P}_v)\mathbf{F}_v\right) \tag{6}$$

To solve Eq. (6), we introduce the following **Theorem 1**.

Theorem 1. *For the following optimization problem, the optimal solution of*

$$\begin{aligned}&\max_{\mathbf{G}} \mathrm{tr}\left(\mathbf{G}^{\mathrm{T}}\mathbf{B}\right) \\ &\text{s.t. } \mathbf{G}^{\mathrm{T}}\mathbf{G} = \mathbf{I},\end{aligned} \tag{7}$$

is $\mathbf{G} = \mathbf{U}[\mathbf{I}, \mathbf{0}]\mathbf{V}^{\mathrm{T}}$, *where* $\mathbf{U}$ *and* $\mathbf{V}$ *are the left-singular vectors and right-singular vectors, produced by singular value decomposition (SVD) on* $\mathbf{B}$.

Proof. From SVD solution $\mathbf{B} = \mathbf{U}\Sigma\mathbf{V}^{\mathrm{T}}$ and together with Eq. (7), it is evident that

$$\begin{aligned}\mathrm{tr}\left(\mathbf{G}^{\mathrm{T}}\mathbf{B}\right) &= \mathrm{tr}\left(\mathbf{G}^{\mathrm{T}}\mathbf{U}\Sigma\mathbf{V}^{\mathrm{T}}\right) = \mathrm{tr}\left(\Sigma\mathbf{V}^{\mathrm{T}}\mathbf{G}^{\mathrm{T}}\mathbf{U}\right) \\ &= \mathrm{tr}\left(\Sigma\mathbf{H}\right)\end{aligned} \tag{8}$$

where $\mathbf{H} = \mathbf{V}^{\mathrm{T}}\mathbf{G}^{\mathrm{T}}\mathbf{U}$, $\Sigma_{i,i}$ and $\mathbf{H}_{i,i}$ are the i-th row and column elements from Σ and $\mathbf{H}$, respectively. We can simply verify $\mathbf{H}\mathbf{H}^{\mathrm{T}} = \mathbf{I}$, where $\mathbf{I}$ is an identity matrix. Consequently, $\Sigma_{i,i} \geq 0$ and $-1 \leq \mathbf{H}_{i,i} \leq 1$. Thus, we have:

$$\mathrm{tr}\left(\mathbf{G}^{\mathrm{T}}\mathbf{B}\right) = \sum_i \Sigma_{i,i}\mathbf{H}_{i,i} \leq \sum_i \mathbf{H}_{i,i}. \tag{9}$$

The equality holds when $\mathbf{H}$ is an identity matrix. Therefore, when $\mathbf{H} = [\mathbf{I}, \mathbf{0}]$, $\mathrm{tr}\left(\mathbf{G}^{\mathrm{T}}\mathbf{B}\right)$ reaches its maximum. Thus, we get the solution of Eq. (6) is: $\mathbf{G} = \mathbf{U}[\mathbf{I}, \mathbf{0}]\mathbf{V}^{\mathrm{T}}$.

Update $\mathbf{F}_v$ with fixed $\{a_v, \mathbf{M}_v, \mathbf{G}_v, \boldsymbol{\mathcal{J}}, \mathbf{W}_{\overline{v}}, \mathbf{A}_v\}$, Eq. (4) becomes:

$$\begin{aligned}\min_{\mathbf{F}_v} &a_v^2 \left\|\mathbf{E}_v + \mathbf{M}_v\mathbf{P}_v - \mathbf{G}_v\mathbf{F}_v^{\mathrm{T}}\right\|_F^2 + \frac{\rho}{2}\left\|\mathbf{F}_v - \mathbf{J}_v + \frac{\mathbf{Y}_v}{\rho}\right\|_F^2 \\ &\text{s.t. } \mathbf{F}_v \geq 0.\end{aligned} \tag{10}$$

And minimizing Eq. (10) is equivalent to

$$\min_{\mathbf{F}_v\geq 0} \left\|\mathbf{F}_v - \frac{a_v^2(\mathbf{E}_v + \mathbf{M}_v\mathbf{P}_v)^{\mathrm{T}}\mathbf{G}_v + \frac{\rho}{2}(\mathbf{J}_v - \frac{\mathbf{Y}_v}{\rho})}{a_v + \frac{\rho}{2}}\right\|_F^2. \tag{11}$$

The solution of Eq. (11) is:

$$\mathbf{F}_v = \left(\frac{a_v^2(\mathbf{E}_v + \mathbf{M}_v\mathbf{P}_v)^{\mathrm{T}}\mathbf{G}_v + \frac{\rho}{2}(\mathbf{J}_v - \frac{\mathbf{Y}_v}{\rho})}{a_v + \frac{\rho}{2}}\right)_+. \tag{12}$$

Update $\mathbf{M}_v$ with fixed $\{a_v, \mathbf{G}_v, \mathbf{F}_v, \mathcal{J}, \mathbf{W}_{\overline{v}}, \mathbf{A}_v\}$, Eq. (4) becomes:

$$\begin{aligned}\min_{\mathbf{M}_v} & a_v^2 \left\|\mathbf{Q}_v + \mathbf{M}_v\mathbf{P}_v\right\|_F^2 + \lambda_2 \left\|\mathbf{W}_{\overline{v}}\mathbf{X}_{\overline{v}} - \mathbf{A}_v\mathbf{M}_v\right\|_F^2 . \\ & \text{s.t. } \mathbf{M}_v^{\mathrm{T}}\mathbf{1} = \mathbf{1}, \mathbf{M}_v \geq 0, \mathbf{W}_{\overline{v}}^{\mathrm{T}}\mathbf{W}_{\overline{v}} = \mathbf{I}, \mathbf{A}_v^{\mathrm{T}}\mathbf{A}_v = \mathbf{I},\end{aligned} \tag{13}$$

where $\mathbf{Q}_v = \mathbf{E}_v - \mathbf{G}_v\mathbf{F}_v^{\mathrm{T}}$. And Eq. (13) can be transformed into following equivalence problem:

$$\min_{\mathbf{M}_v^{\mathrm{T}}\mathbf{1}=\mathbf{1}, \mathbf{M}_v \geq 0} \left\| \mathbf{M}_v - \frac{-a_v^2\mathbf{Q}_v\mathbf{P}_v^{\mathrm{T}} + \lambda_2\mathbf{A}_v^{\mathrm{T}}\mathbf{W}_{\overline{v}}\mathbf{X}_{\overline{v}}}{a_v + \lambda_2} \right\|_F^2 . \tag{14}$$

Eq. (14) is an euclidean projection problem on the simplex space, which has a closed-form solution (Wang, Zhang, and Zhou 2025d).

Update $\mathcal{J}$ with fixed $\{a_v, \mathbf{M}_v, \mathbf{G}_v, \mathbf{F}_v, \mathbf{W}_{\overline{v}}, \mathbf{A}_v\}$, Eq. (4) becomes:

$$\min_{\mathcal{J}} \lambda_1 \left\|\mathcal{J}\right\|_{\circledS}^p + \frac{\rho}{2} \left\| \mathcal{F} - \mathcal{J} + \frac{\mathcal{Y}}{\rho} \right\|_F^2 , \tag{15}$$

which has a closed-form as **Lemma 1** (Gao et al. 2021):

Lemma 1. *Given a third-order tensor $\mathcal{C} \in \mathbb{R}^{n_1 \times n_2 \times n_3}$ and its tensor singular value decomposition $\mathcal{C} = \mathcal{U} * \mathbf{\Sigma} * \mathcal{V}^T$. The optimal solution of*

$$\min_{\mathcal{J}} \beta \left\|\mathcal{J}\right\|_{\circledS}^p + \frac{1}{2} \left\|\mathcal{J} - \mathcal{C}\right\|_F^2 , \tag{16}$$

is $\mathcal{J}^* = \mathcal{S}_\tau(\mathcal{C}) = \mathcal{U} * ifft(\Gamma_\tau(\overline{\mathbf{\Sigma}})) * \mathcal{V}^T$, where $\Gamma_\tau(\overline{\mathbf{\Sigma}})$ is a f-diagonal tensor in Fourier domain, whose diagonal elements can be obtained by using the GST algorithm introduced in (Gao et al. 2021).

By utilizing **Lemma 1**, the solution of $\mathcal{J}$ in Eq. (15) is:

$$\mathcal{S}_{\frac{\lambda_1}{\rho}}(\mathcal{F} + \frac{\mathcal{Y}}{\rho}). \tag{17}$$

Update $\mathbf{A}_v$ with fixed $\{a_v, \mathbf{M}_v, \mathbf{G}_v, \mathbf{F}_v, \mathcal{J}, \mathbf{W}_{\overline{v}}\}$, Eq. (4) becomes:

$$\min_{\mathbf{A}_v^{\mathrm{T}}\mathbf{A}_v = \mathbf{I}} \left\|\mathbf{W}_{\overline{v}}\mathbf{X}_{\overline{v}} - \mathbf{A}_v\mathbf{M}_v\right\|_F^2 , \tag{18}$$

which is equivalent to:

$$\max_{\mathbf{A}_v^{\mathrm{T}}\mathbf{A}_v = \mathbf{I}} \mathrm{tr}\left(\mathbf{A}_v^{\mathrm{T}}\mathbf{W}_{\overline{v}}\mathbf{X}_{\overline{v}}\mathbf{M}_v^{\mathrm{T}}\right) . \tag{19}$$

According to **Theorem 1**, we get the closed-form solution.

Update $\mathbf{W}_{\overline{v}}$ with fixed $\{a_v, \mathbf{M}_v, \mathbf{G}_v, \mathbf{F}_v, \mathcal{J}, \mathbf{A}_v\}$, Eq. (4) becomes:

$$\min_{\mathbf{W}_{\overline{v}}^{\mathrm{T}}\mathbf{W}_{\overline{v}} = \mathbf{I}} \left\|\mathbf{W}_{\overline{v}}\mathbf{X}_{\overline{v}} - \mathbf{A}_v\mathbf{M}_v\right\|_F^2 , \tag{20}$$

which can be written as:

$$\max_{\mathbf{W}_{\overline{v}}^{\mathrm{T}}\mathbf{W}_{\overline{v}} = \mathbf{I}} \mathrm{tr}\left(\mathbf{W}_{\overline{v}}^{\mathrm{T}}\mathbf{A}_v\mathbf{M}_v\mathbf{X}_{\overline{v}}^{\mathrm{T}}\right) . \tag{21}$$

Similarly, Eq.(21) has a closed-form solution as Eq.(19).

Update a_v with fixed $\{\mathbf{M}_v, \mathbf{G}_v, \mathbf{F}_v, \mathcal{J}, \mathbf{W}_{\overline{v}}, \mathbf{A}_v\}$, Eq. (4) becomes:

$$\min_{a_v} \sum_{v=1}^{V} a_v^2 r_v^2 \quad \text{s.t.} a_v \geq 0, \mathbf{a}^\top\mathbf{1} = \mathbf{1}, \tag{22}$$

where $r_v = \left\|\mathbf{E}_v + \mathbf{M}_v\mathbf{P}_v - \mathbf{G}_v\mathbf{F}_v^{\mathrm{T}}\right\|_F$. According to Cauchy-Schwarz's inequality, we can get the optimal solution of a_v by

$$a_v = \frac{\frac{1}{r_v}}{\sum_{v=1}^{V} \frac{1}{r_v}}. \tag{23}$$

Finally, the entire optimization procedure for Eq. (4) is listed in Algorithm 1. The code is available at **https://github.com/W-Xinxin/AGLF**

Algorithm 1: AGLF

Input: Data matrices $\{\mathbf{X}^v\}_{v=1}^V \in \mathbb{R}^{d_v \times (n-n_v)}$, the number of anchors m, the number of clusters k.
Output: Clustering labels of data points.

```
Initialize M_v = 0, G_v = 0, F_v = J_v = 0, Y = 0, W_v̄ = 0, A_v̄ = 0, a_v = 1/V, ρ = 10^-4
Compute graph E_v and construct X_v̄ for each view.
while not converge do
    Update G_v by solving Eq. (6);
    Update F_v by solving Eq. (12);
    Update J by solving Eq. (17);
    Update M_v by solving Eq. (14);
    Update A_v by solving Eq. (19);
    Update W_v̄ by solving Eq. (21);
    Update a_v by Eq. (23);
    Update Y and ρ: Y = Y + ρ(F − J), ρ = min(μρ, 10^12);
end while
Calculate the clustering results by using F = Σ_{v=1}^V a_v^2 F_v / Σ_{v=1}^V a_v^2.
return Clustering result.
```

Convergence Analysis

Our objective function (4) is bounded since it is a sum of various terms with positive norms. The optimization algorithm divides the optimization problem into six sub-procedures, each solving for one variable while keeping the others fixed. Each sub-problem is monotonically decreasing, allowing our algorithm to converge to a local optimum, as supported by the convergence theorem in (Rudin 1976). The empirical results presented in the experiment section demonstrate this point in practice.

Complexity Analysis

Our method consists of two stages: 1) Construction of $\mathbf{E}_v$; 2) using Algorithm 1 to solve Eq. (4). The first stage costs $\mathcal{O}(Vnmd + Vnmlog(m))$, where d is the sum of the feature dimensions on each view. The second stage focuses

on solving $\{\mathbf{M}_v, \mathbf{F}_v, \mathbf{G}_v, \mathcal{J}, \mathbf{W}_{\overline{v}}, \mathbf{A}_v\}$. The complexity for updating these variables iteratively are $\mathcal{O}(Vnmk + \sum_{v=1}^{V} hmn_v d_{\overline{v}} + \sum_{v=1}^{V} mn_v)$,$\mathcal{O}(Vnmk)$, $\mathcal{O}(Vnmk + Vmk^2)$, $\mathcal{O}(2Vnklog(Vk) + V^2kn)$, $\mathcal{O}(\sum_{v=1}^{V} hmn_v d_{\overline{v}} + d_{\overline{v}}h^2)$, and $\mathcal{O}(\sum_{v=1}^{V} hmn_v d_{\overline{v}} + mh^2)$. Due to $m \ll n$, and k, V are small constants, the main computational complexity of solving (4) is $\mathcal{O}(Vnmk + \sum_{v=1}^{V} hmn_v d_{\overline{v}})$. Therefore, the total computational complexity is $\mathcal{O}(Vnmd + \sum_{v=1}^{V} hmn_v d_{\overline{v}})$, highlighting that our method scales well with data size.

Experiments

Datasets and Baselines

We evaluate the performance of our algorithm on six extensively used multi-view datasets: **MSRCv1**, **BDGP**, **Caltech101-7**, **CCV**, **Animal**, and **FMNIST**. The details of these datasets are demonstrated in Table 1.

Datasets	Samples	Cluster	View
MSRCv1	210	7	5
Caltech101-7	1474	7	6
BDGP	2500	5	3
CCV	6773	20	3
Animal	11673	20	4
FMNIST	60000	10	3

Table 1: Description of used multi-view datasets

Following the common approach in (Wang, Zhang, and Zhou 2025b; Wang et al. 2022), we set 9 missing ratios $\omega = [0.1 : 0.1 : 0.9]$ to represent the percentage of samples with incomplete views. When $\omega = 0.1$, we randomly select 10% of the samples to drop partial views, ensuring that at least one view is retained.

Our algorithm is compared with the following incomplete multi-view clustering methods: UEAF (Wen et al. 2019), IMVC-CBG (Wang et al. 2022), FIMVC-VIA (Liu et al. 2022), PIMVC (Deng et al. 2023), CPSCAN (Jin et al. 2023), PSIMVC-PG (Li et al. 2024b), DIVIDE (Lu et al. 2024), PMIMC (Yuan et al. 2025), RISE (Wang, Zhang, and Zhou 2025b). They are introduced in related work.

Implementation Details

For experimental fairness, the hyperparameters for the aforementioned methods are set to the recommended values specified in their original papers. For our model, the parameter λ_1 is searched in $[10^{-2}, 10^{-1}, ..., 10^{2}]$ and the parameter λ_2 is adjusted in $[10^{-5}, 10^{-4}, ..., 10^{5}]$. The traditional models: UEAF, IMVC-CBG, FIMVC-VIA, PIMVC, PSIMVC-PG, and RISE were performed on a computer with a 3.5GHz AMD Ryzen 9 3950x CPU and 64GB of RAM, utilizing MATLAB 2022b (64-bit), while the deep learning models: CPSCAN, DIVIDE, and PMIMC were run on an Ubuntu system with an NVIDIA TITAN RTX GPU.

To evaluate the performance, three widely used clustering metrics: accuracy (ACC), normalized mutual information (NMI), and Purity are used. The higher the values of these metrics, the better the clustering performance. To mitigate the initialization sensitivity of K-means used in several methods, we repeat the experiments 10 times and report the average results.

Anchor Selection and Graph Construction

Our method employs K-means to select anchors from each view and construct anchor graphs $\mathbf{E}_v$ using a parameter-free and effective bipartite graph construct strategy (Li et al. 2020). More details are provided in the appendix.

Performance Comparison

We summarize the results across all missing ratios and report the averages, with the best and second best results marked in Table 2. We can draw the following observations:

1. Our proposed method consistently outperforms all compared methods across three metrics in most circumstances. For example, regarding the ACC metric, it achieves an average improvements of 11.65%, 18.04%, 35.61%, 14.37%, 25.16%, 8.42% over the state-of-the-art across six datasets with missing ratios varying from 0.1 to 0.9. The superiority observed in the other criteria are similar, further demonstrating its outstanding performance across all datasets.
2. Data diversity may exhibit varying clustering patterns, leading to different algorithms performing differently across various datasets. For example, PIMVC achieves the promising results on the MSRCv1, CCV, and Animal datasets, while PMIMC excels on the Caltech101-7 and BDGP datasets. Additionally, RISE shows strong performance on the FMNIST dataset. In contrast, our proposed method consistently demonstrates the best performance across all datasets, indicating the effectiveness of anchor graph learning.
3. By comparing our method with various approaches that do not rely on anchors, such as UEAF and PIMVC, we observe that our proposed method not only achieves superior performance but also effectively handles large-scale dataset, such as FMNIST. In addition, our method outperforms deep learning methods, highlighting its potential for practical applications.

To further evaluate the stability of our model regarding varying missing ratios, we plot the result curves across the varying missing ratios of $[0.1 : 0.1 : 0.9]$. As shown in Figure 1, this visualization allows us to observe how performance changes as the missing ratio increases. When the percentage of incomplete samples increases, most methods experience a decline in performance, while our method exhibits a more stable response. Moreover, our method shows upward trends in performance on the Caltech101-7 and BGDP datasets during certain phases as the missing ratio increases. This indicates the advantages of combining compensation subgraphs from supplementary views.

Parameter Study

Our method involves four parameters that need to be adjusted appropriately, *i.e.*, the trade-off parameters λ_1 and λ_2,

Datasets	Metrics	UEAF AAAI'19	IMVC-CBG CVPR'22	FIMVC-VIA TNNLS'22	PIMVC TNNLS'23	CPSCAN CVPR'23	PSIMVC-PG TNNLS'24	DIVIDE AAAI'24	PMIMC TIP'25	RISE AAAI'25	**Ours**
MSRCv1	ACC	56.23	60.93	74.28	<u>79.56</u>	74.13	60.27	53.50	70.42	71.66	**91.21**
	NMI	45.22	51.20	62.43	<u>69.54</u>	65.60	50.53	42.35	61.26	58.85	**86.96**
	Purity	57.21	61.80	74.33	<u>80.49</u>	75.50	61.34	55.84	72.91	75.47	**91.21**
Caltech101-7	ACC	37.27	59.88	48.60	66.89	54.92	48.52	35.92	47.70	<u>70.72</u>	**88.76**
	NMI	27.89	43.13	44.94	54.09	56.04	42.80	37.59	<u>59.65</u>	53.35	**82.41**
	Purity	77.57	81.03	80.61	86.94	86.76	80.61	76.16	<u>87.36</u>	80.15	**92.58**
BDGP	ACC	44.37	36.06	41.25	30.83	39.96	40.97	33.87	<u>50.85</u>	44.85	**86.46**
	NMI	21.80	14.44	16.87	8.46	15.70	18.33	11.01	<u>28.90</u>	19.22	**83.25**
	Purity	45.41	37.22	41.67	31.97	40.75	43.64	35.68	51.88	<u>61.41</u>	**86.64**
CCV	ACC	14.75	16.77	12.97	<u>20.81</u>	17.23	16.66	18.77	16.06	17.61	**35.18**
	NMI	10.55	13.40	14.90	<u>18.25</u>	14.28	11.76	15.02	13.03	12.30	**49.65**
	Purity	18.75	20.15	22.84	25.27	21.11	19.97	22.01	20.10	<u>29.36</u>	**36.14**
Animal	ACC	17.40	15.51	16.07	<u>19.73</u>	13.04	14.90	15.91	16.01	15.95	**44.89**
	NMI	13.94	11.25	11.31	<u>15.62</u>	8.68	10.65	11.56	15.16	9.77	**59.05**
	Purity	20.83	18.90	19.47	22.21	15.52	18.34	19.24	20.08	<u>32.14</u>	**45.80**
FMNIST	ACC	OM	22.74	20.60	OM	14.77	22.20	10.52	25.13	<u>51.24</u>	**59.66**
	NMI	OM	6.01	4.04	OM	3.42	3.11	3.11	22.70	<u>38.08</u>	**49.12**
	Purity	OM	22.80	21.05	OM	15.78	22.20	10.58	25.23	<u>59.51</u>	**60.62**

Table 2: Average clustering performance of our proposed method and other compared methods on six datasets. 'OM' represents out of memory. The 1st/2nd best results are marked in **bold** and <u>underline</u>.

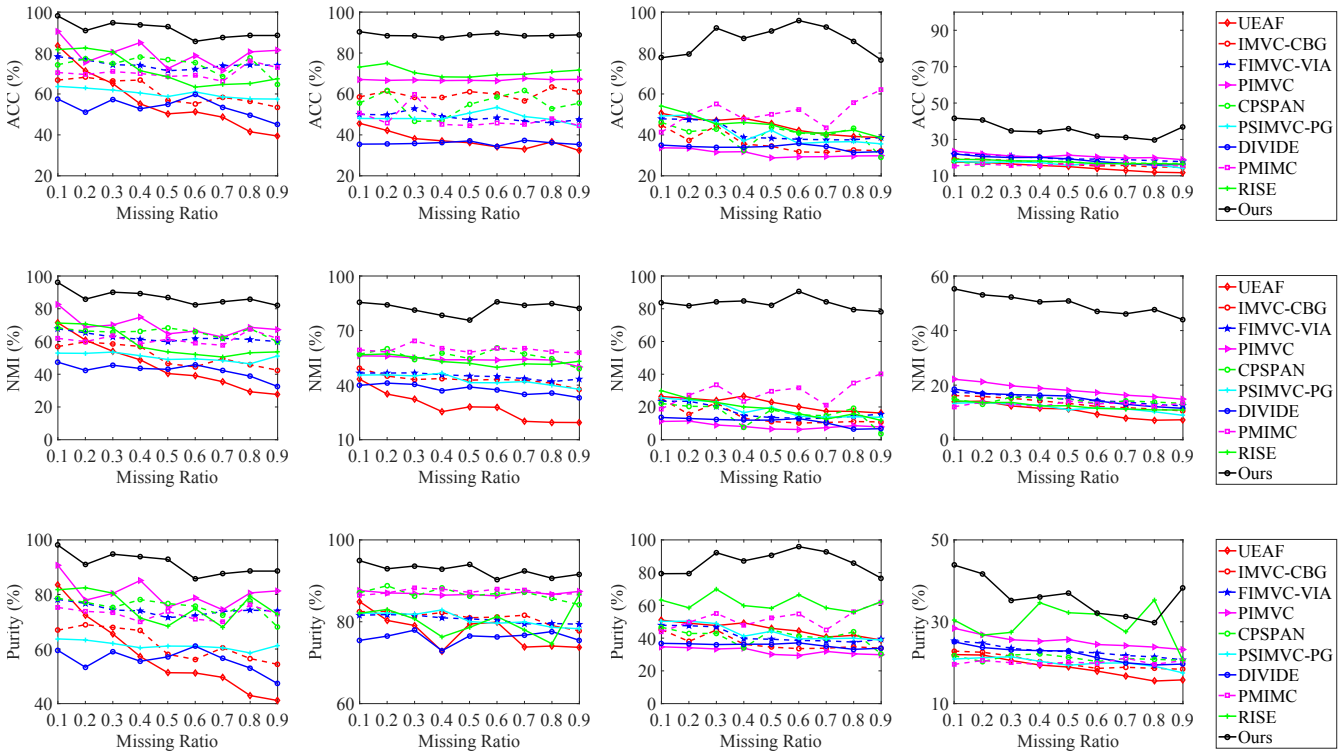

(a) MSRCv1 (b) Caltech101-7 (c) BDGP (d) CCV

Figure 1: The ACC, NMI, and Purity curves under varying missing ratios. The curves on other datasets are similar and we omit them due to space limitations.

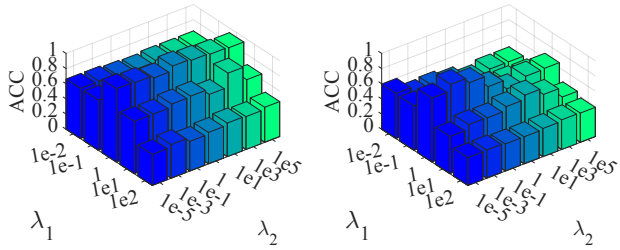

(a) MSRCv1 ($\omega = 0.1$) (b) MSRCv1 ($\omega = 0.5$)

Figure 2: Variation of ACC values with respect to λ_1 and λ_2 on the MSRCv1 dataset for different missing ratios.

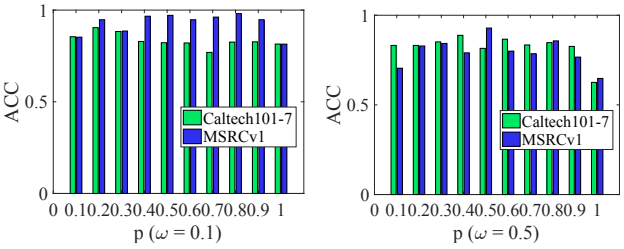

Figure 3: Variation of ACC values with respect to coefficient p across two datasets for different missing ratios.

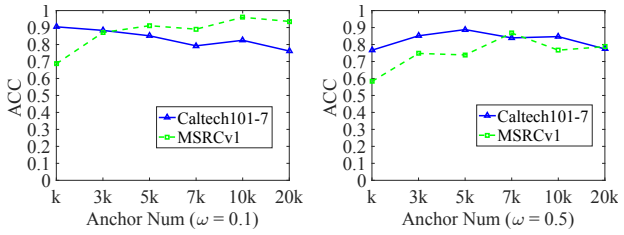

Figure 4: Variation of ACC values with respect to different anchor number on two datasets for different missing ratios.

tensor low rank coefficient p, and the number of anchors used to construct the anchor graphs $\mathbf{E}_v$. We first conduct an experiment on the MSRCv1 dataset with a missing ratio of 0.1 to analyze the sensitivity of λ_1 and λ_2. As shown in Figure 2, we observe that our method achieves satisfactory performance across a wide range of λ_1 and λ_2. To illustrate the effect of missing ratio on the model's sensitivity, we repeat the experiment with a missing ratio of 0.5. The results demonstrate that our model remains relatively stable against changes in the missing ratio.

Figure 3 presents the effects of the parameter p, which is tuned within $p \in \{0.1 : 0.1 : 1\}$. Different values of p affect model performance, with appropriate settings leading to better results. The performance fluctuations are slight across varying missing ratios, demonstrating the model's stability.

Figure 4 demonstrates the impact of the number of anchors. We observe that it is feasible to use a small amount of anchors to achieve promising performance with only slight adjustments, regardless of the missing ratio.

ACC	Miss Ratios		
Models	0.3	0.5	0.7
AGLF w/o CSL	61.43 ($\downarrow_{33.33}$)	53.33 ($\downarrow_{39.53}$)	50.00 ($\downarrow_{37.62}$)
AGLF w/o TS	90.47($\downarrow_{4.29}$)	84.28 ($\downarrow_{8.58}$)	80.95($\downarrow_{6.67}$)
AGLF	94.76	92.86	87.62

Table 3: Ablation study on the MSRCv1 dataset.

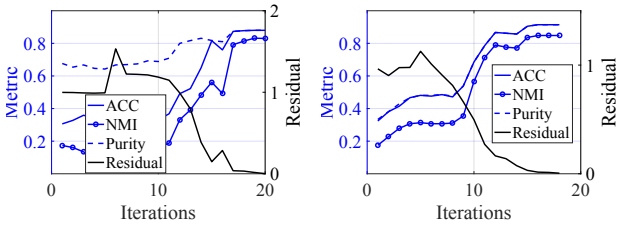

(a) Caltech01-7 (b) MSRCv1

Figure 5: Convergence curves of AGLF on two datasets.

Ablation Study

The compensation subgraph learning is a primary contribution of our model, and the tensor Schatten p-norm is also a key constraint. To assess the effect of these two techniques, we devise two degraded models: "AGLF w/o CSL", which indicates the removal of compensation subgraph learning, and "AGLF w/o TS", which represents substituting the tensor Schatten p-norm with F-norm. The performance comparison is shown in Table 3. We observe that AGLF consistently outperforms the degraded models across varying missing ratios. This indicates these components are essential and effective for our model.

Convergence Study

The proposed algorithm optimizes the objective function iteratively by introducing an auxiliary variable $\mathcal{J}$. Convergence of our algorithm is determined by checking the difference between $\mathcal{J} = \mathcal{F}$. As shown in Figure 5, The difference decreases to nearly zero in fewer than 20 iterations, while three metrics stabilize at high values, demonstrating the effectiveness and practicability of our optimization algorithm.

Conclusion

This paper focuses on exploring cross-view information compensation for incomplete multi-view data, further investigating the complementary information among views. The proposed Cross-view Anchor Graph Learning and Factorization (AGLF) method achieves cross-view structural imputation based on supplementary view data and directly derives soft clustering indicators without the need for post-processing. To solve the proposed objective function, we devise an optimization algorithm based on the Augmented Lagrange Multiplier. Extensive experiments across six datasets demonstrate the effectiveness of our method.

Acknowledgments

This work was supported in part by the Scientific Foundation for Youth Scholars of Shenzhen University (File no. 868-000001033519), by the Guangdong-Macao Science and Technology Innovation Joint Fundation under Grant 2024A0505090003, by the Guangdong Provincial Key Laboratory under Grant 2023B1212060076, and by the Science and Technology Development Fund, Macau SAR (File no. 0050/2024/AGJ, 0049/2022/A1).

References

Chen, Y.; Zhao, X.; Zhang, Z.; Liu, Y.; Su, J.; and Zhou, Y. 2023. Tensor learning meets dynamic anchor learning: From complete to incomplete multiview clustering. *IEEE Transactions on Neural Networks and Learning Systems*, 35(11): 15332–15345.

Cui, J.; Fu, Y.; Huang, C.; and Wen, J. 2022. Low-rank graph completion-based incomplete multiview clustering. *IEEE Transactions on Neural Networks and Learning Systems*, 35(6): 8064–8074.

Deng, S.; Wen, J.; Liu, C.; Yan, K.; Xu, G.; and Xu, Y. 2023. Projective incomplete multi-view clustering. *IEEE Transactions on Neural Networks and Learning Systems*, 35(8): 10539–10551.

Gao, Q.; Zhang, P.; Xia, W.; Xie, D.; Gao, X.; and Tao, D. 2021. Enhanced tensor RPCA and its application. *IEEE transactions on pattern analysis and machine intelligence*, 43(6): 2133–2140.

Hu, S.; Shi, Z.; and Ye, Y. 2022. DMIB: Dual-Correlated Multivariate Information Bottleneck for Multiview Clustering. *IEEE Trans. Cybern.*, 52(6): 4260–4274.

Jin, J.; Wang, S.; Dong, Z.; Liu, X.; and Zhu, E. 2023. Deep incomplete multi-view clustering with cross-view partial sample and prototype alignment. In *Proceedings of the IEEE/CVF conference on computer vision and pattern recognition*, 11600–11609.

Kilmer, M. E.; and Martin, C. D. 2011. Factorization strategies for third-order tensors. *Linear Algebra and its Applications*, 435(3): 641–658.

Li, J.; Gao, Q.; Wang, Q.; and Xia, W. 2024a. Tensorized label learning on anchor graph. In *Proceedings of the AAAI conference on artificial intelligence*, volume 38, 13537–13544.

Li, M.; Wang, S.; Liu, X.; and Liu, S. 2024b. Parameter-free and scalable incomplete multiview clustering with prototype graph. *IEEE Transactions on Neural Networks and Learning Systems*, 35(1): 300–310.

Li, X.; Pan, Y. P.; Sun, Y.; Sun, Q.; Sun, Y.; W. Tsang, I.; and Ren, Z. 2025. Incomplete Multi-view Clustering with Paired and Balanced Dynamic Anchor Learning. *IEEE Transactions on Multimedia*, 27: 1486–1497.

Li, X.; Pan, Y. P.; Sun, Y.; Sun, Q. S.; Tsang, I. W.; and Ren, Z. 2024c. Fast Unpaired Multi-view Clustering. 4488–4496.

Li, X.; Sun, Y.; Sun, Q.; and Ren, Z. 2022a. Consensus cluster center guided latent multi-kernel clustering. *IEEE Transactions on Circuits and Systems for Video Technology*, 33(6): 2864–2876.

Li, X.; Sun, Y.; Sun, Q.; Ren, Z.; and Sun, Y. 2023. Cross-view graph matching guided anchor alignment for incomplete multi-view clustering. *Information Fusion*, 100: 101941.

Li, X.; Zhang, H.; Wang, R.; and Nie, F. 2020. Multiview clustering: A scalable and parameter-free bipartite graph fusion method. *IEEE transactions on pattern analysis and machine intelligence*, 44(1): 330–344.

Li, X.-L.; Chen, M.-S.; Wang, C.-D.; and Lai, J.-H. 2022b. Refining graph structure for incomplete multi-view clustering. *IEEE transactions on neural networks and learning systems*, 35(2): 2300–2313.

Lin, Y.; Gou, Y.; Liu, Z.; Li, B.; Lv, J.; and Peng, X. 2021. Completer: Incomplete multi-view clustering via contrastive prediction. In *Proceedings of the IEEE/CVF conference on computer vision and pattern recognition*, 11174–11183.

Liu, C.; Wen, J.; Wu, Z.; Luo, X.; Huang, C.; and Xu, Y. 2023. Information recovery-driven deep incomplete multiview clustering network. *IEEE Transactions on Neural Networks and Learning Systems*, 35(11): 15442–15452.

Liu, S.; Liang, K.; Dong, Z.; Wang, S.; Yang, X.; Zhou, S.; Zhu, E.; and Liu, X. 2024. Learn from view correlation: An anchor enhancement strategy for multi-view clustering. In *Proceedings of the IEEE/CVF conference on computer vision and pattern recognition*, 26151–26161.

Liu, S.; Liu, X.; Wang, S.; Niu, X.; and Zhu, E. 2022. Fast incomplete multi-view clustering with view-independent anchors. *IEEE Transactions on Neural Networks and Learning Systems*, 35(6): 7740–7751.

Liu, X.; Zhu, X.; Li, M.; Tang, C.; Zhu, E.; Yin, J.; and Gao, W. 2019. Efficient and effective incomplete multi-view clustering. In *Proceedings of the AAAI conference on artificial intelligence*, volume 33, 4392–4399.

Lu, Y.; Lin, Y.; Yang, M.; Peng, D.; Hu, P.; and Peng, X. 2024. Decoupled contrastive multi-view clustering with high-order random walks. In *Proceedings of the AAAI conference on artificial intelligence*, volume 38, 14193–14201.

Qin, Y.; Feng, G.; and Zhang, X. 2025. Scalable One-Pass Incomplete Multi-View Clustering by Aligning Anchors. *Proceedings of the AAAI Conference on Artificial Intelligence*, 39(19): 20042–20050.

Qin, Y.; and Qian, L. 2024. Fast Elastic-Net Multi-view Clustering: A Geometric Interpretation Perspective. In *Proceedings of the 32nd ACM International Conference on Multimedia*, 10164–10172.

Qin, Y.; Zhang, X.; Yu, S.; and Feng, G. 2025. A survey on representation learning for multi-view data. *Neural Networks*, 181: 106842.

Rudin, W. 1976. Principles of mathematical analysis. *3rd ed.*

Wang, J.; Chen, Y.; Wang, Z.; and Zhao, W. 2021. Popularity-enhanced news recommendation with multi-view interest representation. In *Proceedings of the 30th ACM international conference on information & knowledge management*, 1949–1958.

Wang, S.; Liu, X.; Liu, L.; Tu, W.; Zhu, X.; Liu, J.; Zhou, S.; and Zhu, E. 2022. Highly-efficient incomplete large-scale multi-view clustering with consensus bipartite graph. In *Proceedings of the IEEE/CVF conference on computer vision and pattern recognition*, 9776–9785.

Wang, X.; Zhang, Y.; Zhang, J.; and Zhou, Y. 2025. Incomplete Multiview Clustering using Discriminative Feature Recovery and Tensorized Matrix Factorization. *IEEE Transactions on Circuits and Systems for Video Technology*, 35: 10716–10727.

Wang, X.; Zhang, Y.; and Zhou, Y. 2025a. Bidirectional Probabilistic Multi-graph Learning and Decomposition for Multi-view Clustering. *IEEE Transactions on Image Processing*, 34: 3609–3621.

Wang, X.; Zhang, Y.; and Zhou, Y. 2025b. Highly efficient rotation-invariant spectral embedding for scalable incomplete multi-view clustering. In *Proceedings of the AAAI Conference on Artificial Intelligence*, volume 39, 21312–21320.

Wang, X.; Zhang, Y.; and Zhou, Y. 2025c. Multimodal Remote Sensing Image Clustering with Multi-scale Spectral-Spatial Anchor Graphs. *IEEE Transactions on Geoscience and Remote Sensing*, 63: 1–12.

Wang, X.; Zhang, Y.; and Zhou, Y. 2025d. Pseudo-Supervision Affinity Propagation for Efficient and Scalable Multiview Clustering. *IEEE Transactions on Neural Networks and Learning Systems*, 36: 15282–15293.

Wen, J.; Liu, C.; Xu, G.; Wu, Z.; Huang, C.; Fei, L.; and Xu, Y. 2023a. Highly confident local structure based consensus graph learning for incomplete multi-view clustering. In *Proceedings of the IEEE/CVF conference on computer vision and pattern recognition*, 15712–15721.

Wen, J.; Xu, G.; Tang, Z.; Wang, W.; Fei, L.; and Xu, Y. 2023b. Graph regularized and feature aware matrix factorization for robust incomplete multi-view clustering. *IEEE Transactions on Circuits and Systems for Video Technology*, 34(5): 3728–3741.

Wen, J.; Yan, K.; Zhang, Z.; Xu, Y.; Wang, J.; Fei, L.; and Zhang, B. 2020a. Adaptive graph completion based incomplete multi-view clustering. *IEEE Transactions on Multimedia*, 23: 2493–2504.

Wen, J.; Zhang, Z.; Xu, Y.; Zhang, B.; Fei, L.; and Liu, H. 2019. Unified embedding alignment with missing views inferring for incomplete multi-view clustering. In *Proceedings of the AAAI conference on artificial intelligence*, volume 33, 5393–5400.

Wen, J.; Zhang, Z.; Zhang, Z.; Fei, L.; and Wang, M. 2020b. Generalized incomplete multiview clustering with flexible locality structure diffusion. *IEEE transactions on cybernetics*, 51(1): 101–114.

Wen, J.; Zhang, Z.; Zhang, Z.; Zhu, L.; Fei, L.; Zhang, B.; and Xu, Y. 2021. Unified tensor framework for incomplete multi-view clustering and missing-view inferring. In *Proceedings of the AAAI conference on artificial intelligence*, 10273–10281.

Xia, W.; Gao, Q.; Wang, Q.; and Gao, X. 2022. Tensor completion-based incomplete multiview clustering. *IEEE Transactions on Cybernetics*, 52(12): 13635–13644.

Yuan, H.; Sun, Y.; Zhou, F.; Wen, J.; Yuan, S.; You, X.; and Ren, Z. 2025. Prototype matching learning for incomplete multi-view clustering. *IEEE Transactions on Image Processing*, 34: 828–841.

Zhang, Y.; Wang, S.; Liu, J.; Yu, S.; Dong, Z.; Liu, S.; Liu, X.; and Zhu, E. 2025a. DLEFT-MKC: Dynamic Late Fusion Multiple Kernel Clustering with Robust Tensor Learning via Min-Max Optimization. In *The Thirteenth International Conference on Learning Representations*.

Zhang, Y.; Wang, X.; Jiang, X.; Zhang, L.; and Du, B. 2025b. Elastic Graph Fusion Subspace Clustering for Large Hyperspectral Image. *IEEE Transactions on Circuits and Systems for Video Technology*, 35: 6300–6312.

Zhang, Y.; Yan, S.; Zhang, L.; and Du, B. 2024. Fast projected fuzzy clustering with anchor guidance for multimodal remote sensing imagery. *IEEE Transactions on Image Processing*, 33: 4640–4653.